JCTC Journal of Chemical Theory and Computation

pubs.acs.org/JCTC Article

# Assessing the Intestinal Permeability of Small Molecule Drugs via Diffusion Motion on a Multidimensional Free Energy Surface

Alyson Shoji, Christopher Kang, Kazuumi Fujioka, John P. Rose, and Rui Sun*

Cite This: *J. Chem. Theory Comput.* 2022, 18, 503−515 Read Online

ACCESS | Metrics & More | Article Recommendations | Supporting Information

**ABSTRACT:** A protocol that accurately assesses the intestinal permeability of small molecule compounds plays an essential role in decreasing the cost and time in inventing a new drug. This manuscript presents a novel computational method to study the passive permeation of small molecule drugs based on the inhomogeneous solubility-diffusion model. The multidimensional free energy surface of the drug transiting through a lipid bilayer is computed with transition-tempered metadynamics that accurately captures the mechanisms of passive permeation. The permeability is computed by following the diffusion motion of the drug molecules along the minimal free energy path found on the multidimensional free energy surface. This computational method is assessed by studying the permeability of five small molecule drugs (ketoprofen, naproxen, metoprolol, propranolol, and salicylic acid). The results demonstrate a remarkable agreement between the computed permeabilities and those measured with the intestinal assay. The *in silico* method reported in this manuscript also reproduces the permeability measured from the intestinal assay (*in vivo*) better than the cell-based assays (e.g., PAMPA and Caco-2) do. In addition, the multidimensional free energy surface reveals the interplay between the structure of the small molecule and its permeability, shedding light on strategies of drug optimization.

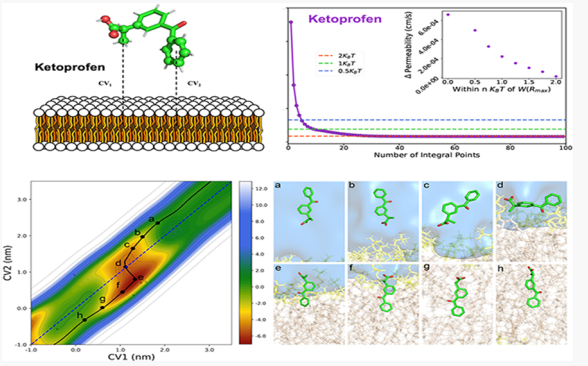




## 1. INTRODUCTION

Small, synthetic organic molecules (i.e., molecular weight less than a few hundred Daltons) account for about 90% of the commercially available pharmaceutical drugs;[1] for example, in 2014, 17 of the top 20 most prescribed drugs in the U.S. were small molecule drugs. In comparison to biomolecules, including peptides and oligomers such as siRNA, small molecules are more chemically stable and much more permeable through biological membranes, allowing them to be administered orally.[2−4] The intestinal region, which has the largest surface area in the human gastrointestinal tract, is the main target for absorption of small molecule drugs.[5] The primary mechanism of intestinal absorption of small molecule drugs is mediated by passive permeation (i.e., concentration gradient driven mass transport) through the membranes of the enterocyte cells that line the intestinal tract.[6] Therefore, a good understanding of the passive permeation of small molecule drugs is of great interest to the pharmaceutical industry. Furthermore, an *in silico* method that is able to screen a large number of small molecule compounds and also shed light on the dependency between the structure of the molecule and permeability mechanism can play a pivotal role in decreasing the cost and time of discovering and developing a new drug.

The passive permeation of small molecules through membranes has been studied extensively both *in vitro* and *in vivo* (e.g., two recent review articles[7,8]). Typically, *in vitro* studies employ a system with two chambers, donor and acceptor, separated by a thin layer that mimics the biological membrane. The two most used *in vitro* assays are (1) cell-based assays, where the permeation layer is a live membrane, such as the Madin−Darby Canine Kidney (MDCK)[9] cells or the heterogeneous human epithelial colorectal adenocarcinoma cells (Caco-2),[10] and (2) an artificial membrane assay where the permeation barrier is some thin lipid layer, such as the parallel artificial membrane permeation assay (PAMPA).[11] Both systems have been widely adopted by both academia as well as the pharmaceutical industry over the past 30 years despite the fact that it is well recognized that *in vitro* permeability is not a reliable measure of *in vivo* permeability and thus human oral absorption cannot be accurately predicted from one single *in vitro* permeability measurement.[12] The shortcomings associated with *in vitro* methods include adsorption onto surfaces of the experimental chamber, potential leakage through paracellular pathways,[13] unphysiological phases formed in PAMPA,[14] and others.[15] These limitations unavoidably decrease the reproducibility of *in vitro*

**Received:** July 1, 2021
**Published:** December 1, 2021

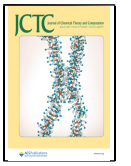

experiments and in turn the reliability of *in vitro* permeability as a measure of *in vivo* permeability and will be further addressed later in the manuscript. In regard to *in vivo* studies, the permeability of small molecule drugs is measured by regional intestinal perfusion techniques.[16,17] Several clinical tools have been developed, all of which are intrusive and involve inserting some kind of a multitube into the jejunum.[18] Briefly, in these methods two balloons are inserted into the lumen to occlude a segment of the intestine, usually the jejunum. Drug-containing solution is injected into this region and the difference between the input and output perfusate concentrations is measured. The passive permeability of a drug is estimated based on the drug loss relative to the estimated surface area of the occluded jejunal segment.[17] In comparison to *in vitro* methods, *in vivo* methods show far superior correlation to human oral absorption; however, there is much less *in vivo* permeation data available as the experiments are far more expensive and intrusive on the subject. Despite their differences, both *in vitro* and *in vivo* methods have revealed correlations between the structure of the small molecule drug and the rate and extent of oral absorption. This correlation has significantly contributed to the development of a "rule of thumb" for evaluating whether a chemical compound has certain chemical and physical properties that would likely make it an orally active drug (e.g., Lipinski's rule of five).[19] However, there are many exceptions to Lipinski's rule of five,[20,21] indicating that more complicated models are necessary for estimating the passive permeation of small molecules.

In contrast to *in vivo* and *in vitro* studies, *in silico* studies approach the passive permeation of small molecule drugs with models and simulations. Molecular dynamics (MD) simulations are one of the most commonly used *in silico* methods to study biophysical processes and are particularly useful in the study of permeation.[22] Numerous MD methods have been developed to compute the free energy of permeation, $W(R)$, and the diffusivity of a small molecule drug, $D(R)$.[22−27] These two quantities can be used to calculate the permeability ($P$) according to the inhomogeneous solubility-diffusion model.[28−30] Developed from the steady-state flux, this model assumes diffusion of the drug during the permeation and takes into account the fact that the diffusivity of the drug varies with respect to its position relative to the bilayer. According to this model, the inverse of the permeability is computed as

$$\frac{1}{P} = \int \frac{\exp[\beta W(R)]}{D(R)} \mathrm{d}R \tag{1}$$

$R$ is a coordinate along the path of the permeation, usually defined as the scaled relative (center of mass) position of the permeant with respect to the lipid bilayer; for example, positions $R = 0$ and $R = 1$ represent the drug molecule on opposite sides outside the lipid bilayer, while $R = 0.5$ represents the drug at the center of the lipid bilayer. Various MD enhanced sampling methods such as umbrella sampling,[31] metadynamics,[32] adaptive biasing force,[33] and etc., have been employed to compute $W(R)$, and their performances are generally comparable.[34] With regard to the diffusivity, $D(R)$, although its physical interpretation remains debatable, e.g., diffusion versus subdiffusion,[27] there have been several methods that are able to estimate the diffusivities of small molecule drugs.[25] Importantly, in addition to estimating the passive permeability, MD simulations can also shed light on the mechanism of passive permeation at an atomistic or molecular level, potentially leading to solutions for overcoming the limitations of Lipinski's rule of five.

Like many computational-based methods, MD simulations of the passive permeation of small molecule drugs suffer from inconsistent agreement with experimental observations.[24−26] For example, the permeabilities of urea, benzoic acid, and codeine were computed with various enhanced sampling MD and resulted in a variation within 1.5 log units (~30-fold difference) of experimental values.[25] Bennion et al.[35] employed umbrella sampling to study the permeation of a range of compounds, and their results differed from *in vitro* results by about 5.0 log units (~$10^5$-fold difference). Several factors to varying degrees can contribute to these large differences: (1) the inaccuracy of the force field, (2) the error associated with the convergence of the enhanced sampling MD, (3) the uncertainty introduced in the calculation of diffusivity, (4) the oversimplified model of the lipid bilayers, and (5) the protonation/deprotonation of the small molecule drug. It is well-known that the permeability calculation is very sensitive to (1) and (2) as they dictate the quality of the free energy of the permeation, $W(R)$, which is scaled exponentially in eq 1. Error related to the diffusivity (factor 3) arises from the different methods of computing $D(R)$, but since $D(R)$ is scaled linearly in eq 1, it is unlikely to be the source of the error that is of a few orders of magnitude in size.[25] With regard to the structure and composition of the membranes (factor 4), even though some efforts have been made to mimic a heterogeneous lipid bilayer,[23] the membranes employed in MD simulations remain far from physiological conditions (lack of curvature, lipid diversity, phase behavior, etc.). Finally for the ionization state of the drug molecule (factor 5), it is very difficult for charged species to passively permeate through a lipid bilayer.[36−38] Therefore, according to its p$K_a$ value (e.g., propranolol, p$K_a$ = 9.5), there could be less than 1% of the molecules in the neutral form when solvated in bulk water, but this less than 1% is favored to partition into the lipid bilayer and eventually permeate. To address this issue, specialized MD, i.e., constant pH, simulations with the ability to model protonation/deprotonation is necessary,[39,40] and a pioneer research paper on this subject can be found in ref 41. The above discussion on the pitfalls of MD simulations leads to the realization: it remains very challenging to directly compare permeabilities of small molecule drugs calculated from simulations to those from experiments. Particularly, an agreement between the gold standard (*in vivo* permeability) and a testing method (*in vitro* or *in silico*) within 1 order of magnitude is considered to be state-of-the-art.[25,42]

This manuscript aims to improve the accuracy and reliability of MD simulations in predicting passive permeabilities by targeting the first three of the five issues mentioned in the previous paragraph. To address the inaccuracy of the force field (no. 1), the partial charges of the small molecule drug will be reparametrized when deemed necessary.[43] With regard to the convergence of the free energy calculation (no. 2), transition-tempered metadynamics, an enhanced sampling method that efficiently and reliably computes the multidimensional free energy of the permeation of small molecule drugs, is utilized.[44] Further, two collective variables (CVs) that characterize the relative position and orientation of the drug with respect to the bilayer are employed. Traditionally, the center of mass distance between the drug and bilayer has been employed as the sole CV in the permeability calculation,[25,34,35] but the inclusion of the additional orientational CV assists the convergence of the


https://doi.org/10.1021/acs.jctc.1c00661
J. Chem. Theory Comput. 2022, 18, 503−515

free energy calculation.[45,46] This additional orientational CV also describes the diffusion motion (no. 3) of the small molecule along the minimal free energy path of the permeation much more accurately. For example, as shown later in the manuscript, the small molecule drug is largely in a "locked" orientation near the water−bilayer interface, thus the additional orientational CV enables the characterization of the diffusion while holding the drug in the favored orientation.[45,46] In addition, the inhomogeneous solubility-diffusion model[28−30] is re-examined, and a computationally more efficient model is proposed, where only the major permeation barriers instead of the entire minimal free energy path are considered. The passive permeation of five small molecule drugs (ketoprofen, naproxen, metoprolol, propranolol, and salicylic acid) are studied in this manuscript, and their *in silico* permeabilities show very good agreement to those measured with the intestinal assay (*in vivo*). It is important to acknowledge that the complexity of the bilayer and the protonation of the drug molecule (issue nos. 4 and 5) also impact the reliability of the *in silico* permeability; nonetheless, the aforenoted methodology improvement can be applied to any lipid bilayer and protonated/deprotonated drug molecules.

The manuscript is organized as follows: the methodology section briefly introduces the method of computing the multidimensional free energy of permeation and diffusivity [$W(R)$ and $D(R)$ in eq 1], the setup of the MD simulation, and a protocol of reparameterizing the partial charge of a small molecule drug. The Results section reports the analysis of transition-tempered metadynamics simulations and the diffusivity calculations and eventually the prediction of the permeabilities. This manuscript concludes with a discussion comparing the *in silico* results to the permeability measured with the intestinal assay (*in vivo*), which is considered to be the most reliable indicator to the bioavailability of a drug molecule.

## 2. METHODOLOGY

**2.1. Multidimensional Free Energy of Passive Permeation, *W*(*R*): Transition-Tempered Metadynamics.** Metadynamics (MetaD) adds bias energy to an $n$-dimensional space defined by collective variables ($CV_1$, $CV_2$, ⋯, $CV_n$), in which $CV_i$ is transformed from coordinates of the system of $N$ atoms, $Q \in \mathbb{R}^{3N}$, through a function $s_i$, i.e., $CV_i = s_i(Q)$.[47] CVs are chosen to represent the transition of the system, e.g., protein folding, substrate binding, etc., which is rare/slow. At every $\tau$th MD integration step, a Gaussian-shaped bias energy is added to the Hamiltonian of the system. The $k$th Gaussian-shaped bias energy is centered at:

$$\begin{aligned}\vec{S}(k\tau) &= (CV_1(k\tau), CV_2(k\tau), ..., CV_n(k\tau)) \\ &= (s_1(Q(k\tau)), s_2(Q(k\tau)), ..., s_n(Q(k\tau))) \in \mathbb{R}^n\end{aligned} \tag{2}$$

in which $\vec{S}$ is the time evolution of the system in the $n$-dimensional space of CVs (i.e., CV space). At time $t$ (assume $(k-1)\tau < t < k\tau$), the system $Q(t) \rightarrow \vec{S}(t)$ is experiencing the bias energy $V_G$ computed as

$$V_G(\vec{S}(t), t) = \sum_{j<t/\tau} w \times \exp\left(-\sum_{i=1}^{n} \frac{(s_i(Q(j\tau)) - s_i(Q(t)))^2}{2\sigma_i^2}\right) \tag{3}$$

in which $w$ and $\sigma_i$ are defined as the height and width of the Gaussian bias along the $i$th CV, respectively. Due to the bias energy, the system is discouraged from revisiting the regions in the CV space that have been visited previously and instead explores regions that have not yet been sampled. After some time $t_D$, the bias energy $V_G$ eventually offsets the underlying free energy surface, making the system move in the CV space in a diffusive and ergodic fashion.[32,48] The estimate of the free energy surface of the system is the time average of $VG(\vec{S}(t),t)$ over $t > t_D$.

In MetaD, the bias energy is added to the system at a constant rate (i.e., $w/\tau$) regardless of the progress of the simulation. It is important to note that the constant energy inflow has been reported to contribute to false convergence and instability of the simulation.[46,49] In response, well-tempered MetaD (WTMetaD) was proposed, which tempers the height of the Gaussian exponentially with respect to the local bias energy $V_G(\vec{S}(t),t)$.[50,51] For example, $w$ in eq 3 is replaced by $w(t)$, which is computed as

$$w(t) = w \cdot \exp\left(-\frac{V_G(\vec{S}(t), t)}{k_B \Delta T}\right) \tag{4}$$

$\Delta T$ is called the bias factor that tempers the height of the Gaussian ($w$), and it should neither temper too early (i.e., the exploration of the CV space would be delayed due to being stuck in a local minima) nor too late (i.e., the bias energy does not converge). $\Delta T$ is suggested to ensure that $(\Delta T + T)k_B$ is close to the highest free energy barrier in the CV space.[52] However, the barrier height is usually the very quantity to be sought, and previous experience has shown a poor estimate of $\Delta T$ could dramatically decrease the efficiency and reliability of WTMetaD.[53,54]

In contrast to WTMetaD, transition-tempered metadynamics (TTMetaD)[44] seeks a balance between the exploration of the CV space and the convergence of the bias energy. Instead of estimating the height of the free energy barrier, TTMetaD requires the user to estimate the position of the minima on the free energy surface, a requirement that is usually easier to fulfill. In TTMetaD, a transition path in the $n$-dimensional CV space is defined as the trace of $\vec{S}(t)$, starting from one of the minima, that connects all the predetermined minima. TTMetaD adds the bias energy to the system the same way as MetaD does, then tempers the height $w$ as soon as at least one such transition path is found. The height of the Gaussian in TTMetaD is defined as follows:

$$w(t) = w \times \exp\left(-\frac{\min[V^*(t)]}{k_B \Delta T}\right) \tag{5}$$

When there are multiple transition paths, the maximally biased one is identified. The minimum bias on this maximally biased path is defined as $V^*(t)$ in eq 5.[44] Observing at least one transition path indicates that the wells in the free energy surface are roughly filled, then TTMetaD tempers the height of the Gaussian aggressively. It is designed to explore the CV space at a fast rate (MetaD-like) and still converges asymptotically (WTMetaD-like). Previous research has shown that TTMetaD is an ideal enhanced sampling method to study the passive permeation of small molecule drugs.[45,46]

In a majority of the previous *in silico* studies,[22−26] a change in $R$ in eq 1 represents the center of mass translation between the small molecule drug and the lipid bilayer, i.e., $R$ = C. M. (drug) − C. M. (lipid) $\in \mathbb{R}$. Recently, Sun et al.[46] have shown that the orientation of the small molecule


https://doi.org/10.1021/acs.jctc.1c00661
J. Chem. Theory Comput. 2022, 18, 503−515

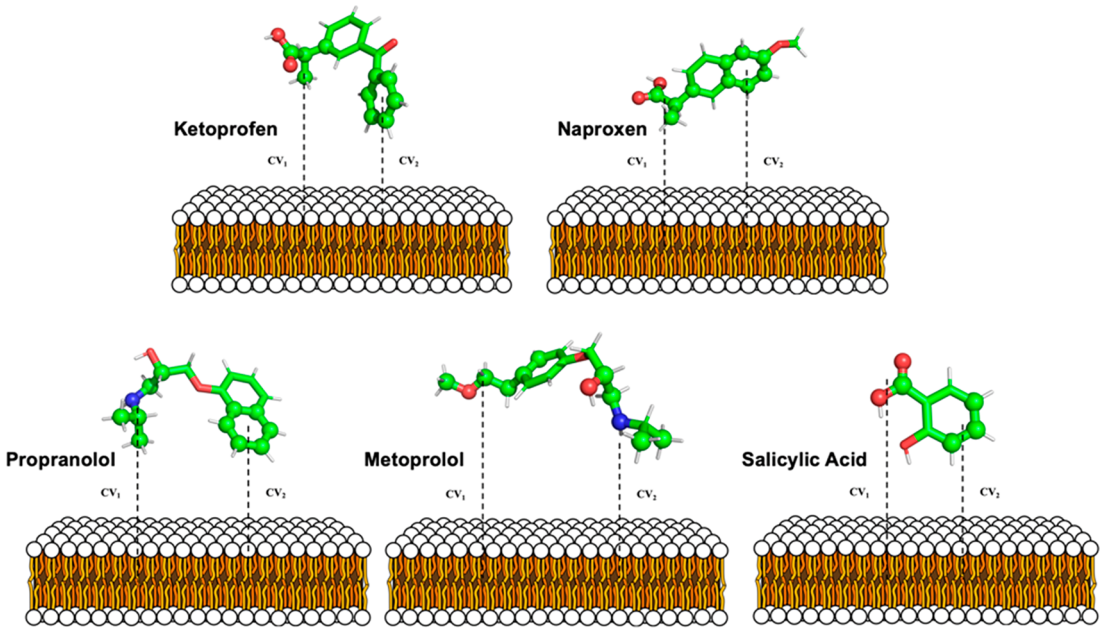


**Figure 1.** Illustrations of the collective variables. For each small molecule drug, the centers of mass are calculated for two select groups of atoms (marked as balls), and they are designated as the terminal ends of the molecule. The distances between each of the terminal ends to the center of mass of the lipid bilayer are employed as collective variables in the TTMetaD simulations.

drug could have a significant impact on its interaction with the lipid bilayer. A new path $R$ that includes this degree of freedom improves the efficiency and reliability of the calculation of $W(R)$. Therefore, $R \in \mathbb{R}^2$ is adopted for this study and is defined by two CVs depicted in Figure 1. The relative position and orientation between the small molecule drug and the lipid can be identified with the average value of the two CVs and the differences between them, respectively. Similar to Sun et al.,[45,46] $R$ is the minimum free energy path (MFEP) calculated from the string method at zero Kelvin.[55] The origin and the end of $R$ represent the drug molecule on opposite sides outside the lipid bilayer, thus a full transition along $R$ indicates a full permeation event. The free energy of the passive permeation, $W(R)$, is evaluated from $V_G(R)$ after the TTMetaD simulation converges.

**2.2. Diffusivity of the Permeant, *D*(*R*): Two-Dimensional Umbrella Sampling.** The diffusivity, $D(R)$, characterizes the speed of the diffusion of the small molecule drug along the MFEP. To calculate $D(R)$, a series of two-dimensional umbrella sampling simulations[31] are prepared, in each of which the small molecule drug is restrained to different points along $R$ (corresponding to different values of $CV_1$ and $CV_2$). For each simulation, the time evolution of the system in the CV space, $\vec{S}(t)$, is orthogonally projected onto the MFEP. The arc length between this projected point and the origin of $R$ is denoted as $l(t) \in \mathbb{R}$. $l(t)$ is collected from the simulation, and $D(R)$ is computed as[56]

$$D(R) = \frac{[\sigma^2(l)]^2}{\int_0^\infty C_l(t)\mathrm{d}t} \tag{6}$$

$\sigma^2(l)$ and $C_l(t)$ are the variance and the autocorrelation function of $l(t)$, respectively. $C_l(t)$ is computed as

$$C_l(t) = \frac{\Delta t}{t_s - t} \sum_{i=1}^{(t_s - t)/\Delta t} (l(i \times \Delta t) - \bar{l}) \times (l(i \times \Delta t + t) - \bar{l}) \tag{7}$$

in which $t_s$ is the length of the umbrella sampling MD after initial equilibration, $\Delta t$ is the MD integration time step, and $\bar{l}$ is the average of $l(t)$ over $t_s$.

Hummer et al. and Woolf et al. have shown that the diffusivity calculated with umbrella sampling MD is independent of the force constant of the harmonic potential, as long as it overwhelms the underlying potential energy of the system.[56,57] As a result, a relatively large force constant, 1913 kcal/(mol/Å$^2$) [i.e., 800,000 kJ/(mol/nm$^2$)], is purposely chosen to confine the sampling of $\vec{S}(t) \in \mathbb{R}^2$ to a relatively small area in the CV space, which enhances the accuracy and reliability of the $\vec{S}(t) \rightarrow l(t)$ projections (from a random point in the two-dimensional CV space to the one-dimensional MFEP in this space). A more detailed description of generating $l(t) \in \mathbb{R}$ from $\vec{S}(t)$ can be found elsewhere.[45]

**2.3. Details of the Molecular Dynamics Simulation.** The lipid bilayer in this research is composed of two leaflets of 16 POPC molecules each. The lateral dimension of the bilayer (i.e., $x$−$y$ plane) is approximately 3.3 × 3.3 nm, a size that has been shown to be large enough for the permeation of small molecule drugs.[46,45] The bilayer is solvated with a hydration ratio of 80 (total of 2560 water molecules, making the $z$ dimension 11.1 nm), and periodic boundary conditions are enforced in every direction. One small molecule drug is solvated into the system. CHARMM36,[58] CHARMM general force fields (CGenFF),[43] and TIP3[59] force fields are used to model the lipids, small molecule drugs, and water molecules, respectively. The Nose-Hoover thermostat[59] is applied to the system at physiological temperature (310 K) and the semi-isotropic Parrinello−Rahman barostat[60] is applied to hold the system at 1.0 bar. The hydrogen bonds are constrained by the linear constraint solver (LINCS),[61] and the MD integration time step is 2 fs. The configurations are set up using the CHARMM-GUI membrane builder,[62] and the MD simulations are carried out using GROMACS-2019.2[63] patched with PLUMED2.4[64] (including TTMetaD[44] developed by the Voth research group). For every small molecule drug, five


https://doi.org/10.1021/acs.jctc.1c00661
J. Chem. Theory Comput. 2022, 18, 503−515

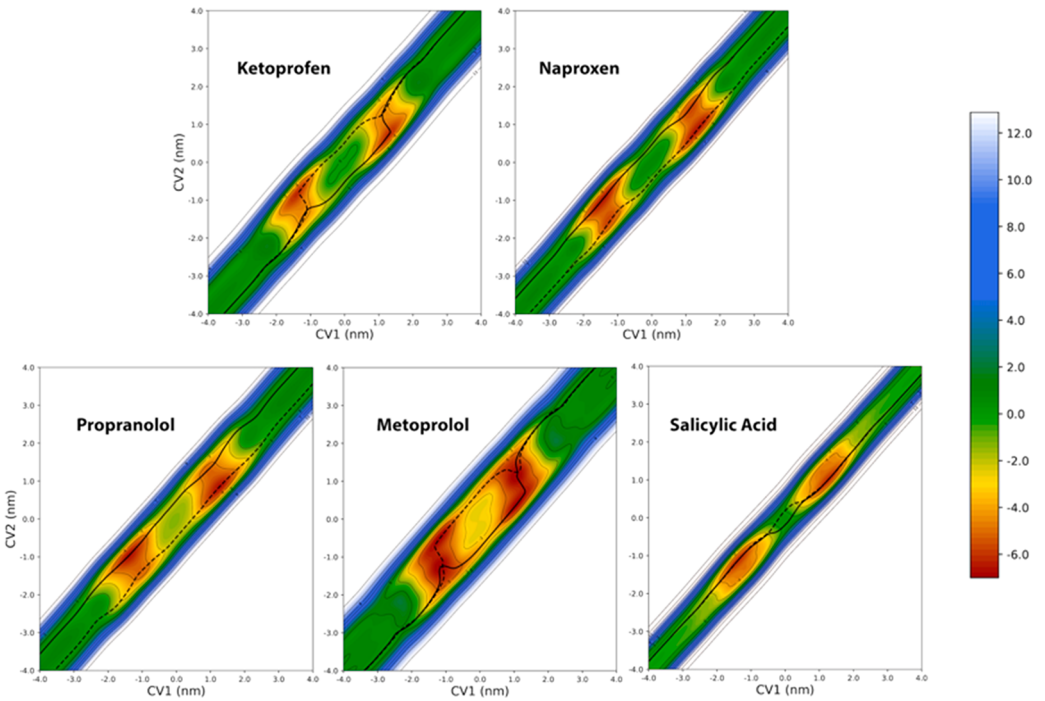


**Figure 2.** Two-dimensional free energy surface for the permeation of five small molecule drugs through a POPC bilayer. The CVs are defined in Figure 1. The unit of the free energy is kcal/mol. The black, solid curves denote the MFEP of the permeation. The dashed curve is the central symmetry image of the solid curve. For more information regarding the dashed curve, please refer to Figure S5.

one-microsecond replicas of TTMetaD simulations are carried out to reach diffusive motion (see Figure S1 for an example) and $W(R)$ is calculated from the ensemble average (see Section 3.1). These replicas start from the same initial configuration, but the velocities of the atoms are randomly generated from a Boltzmann distribution. The Gaussian bias energy deposition rate is every 500 steps with a height of 0.015 kcal/mol and a width of 0.22 nm. The height of the Gaussian is tempered with a bias factor of 10 (i.e., $\Delta T$ in eq 5). The TTMetaD wells are located at (0.0, 0.0) and (0.48, 0.48) in reduced CV coordinates, and the bias threshold is 6.0 kJ/mol (refer to the Supporting Information for more details). The two-dimensional umbrella sampling is also carried out with the same computer program. The small molecule drug is first pulled to the desired position with the "MOVINGRESTRAINT" function in PLUMED and then restrained by a harmonic bias for a total of 200 ns. To make sure the system is fully relaxed, the autocorrelation function is collected from only the last 100 ns. The total simulation time for this research exceeds 26 $\mu$s.

**2.4. Reparameterization the Partial Charges.** The CHARMM General Force Field[43] parameters for the small molecule drugs are generated through a program distributed by SILCSBIO, LLC, freely available to academic researchers. The input of the executable is the structure of the molecule, and the output contains force field parameters assigned according to chemically similar structural motifs in the CGenFF database. A penalty score associated with each of the parameters indicating the level of uncertainty is also printed out. In accordance with CGenFF,[43] a penalty score of less than 10 indicates that the analogy pairing is "fair", between 10 and 50 requires self-validation to determine whether the analogy is appropriate, and anything above the score of 50 means that the analogy is poor and optimization of the molecule is recommended. In this manuscript, only the partial charges are reparameterized when necessary. A brief introduction of the procedure is listed as follows.

*2.4.1. Step 1.* Assign partial charges according to MP2 calculations. The geometry of the molecule is optimized in Gaussian[65] at the MP2/6-31G(d)[66,67] level of theory. Merz−Kollman charges from the MP2 geometry optimization are used to update the initial partial charges from CGenFF (of high penalty) while following the standard CHARMM all-atom force field convention.[68]

*2.4.2. Step 2.* Identify benchmark interaction energies with Hartree-Fock.[69] The interaction energy between every atom (of the small molecule that could form a hydrogen bond) and water is calculated with Hartree-Fock restrained geometry optimization. For compliance with CHARMM, 6-31G(d) basis sets are used, and the water molecule holds a TIP3 structure. One water molecule is aligned linearly with the atom of interest (atom X), and the interaction energy between H−X (if X is a proton acceptor) or O−X (if X is a proton) is calculated with a restrained geometry optimization: only the distance between H−X or O−X is subject to variation while all else remains fixed. The optimized distances and interaction energies are then scaled following the CHARMM all-atom force field convention and used as the benchmark data.

*2.4.3. Step 3.* Fit the partial charges (initially from step 1) to match the benchmark interaction energies from step 2. The molecular mechanics (MM) interaction energies are calculated with the partial charge adjusted to match the benchmark. The standard CHARMM all-atom force field convention is still strictly observed in this step.

It is important to note that Vanommeslaeghe et al.[43] have developed a full parametrization of all force field parameters (i.e., partial charges, van der Waals, bond, angle, dihedral, etc.) involved in a small molecule, and the presented procedure of refitting the partial charges is derived from Vanommeslaeghe et al.[43] This manuscript focuses on only the partial charges for


https://doi.org/10.1021/acs.jctc.1c00661
J. Chem. Theory Comput. 2022, 18, 503−515

two reasons: first and foremost, the partial charges dictate the hydrophobicity of the small molecule and, therefore, largely contribute to the free energy of permeation ($W(R)$) that dominates the estimated permeability. In addition, reparametrizing all force field parameters entails many iterations of QM and MM calculations. It would go against the purpose of this manuscript which is to develop an efficient *in silico* method that screens the permeability of a large set of molecules. Among the five small molecule drugs, only propranolol's partial charges are reparameterized due to their large uncertainties. The results of the charge reparameterization are summarized in Table S1 and Figure S2.

## 3. RESULTS

**3.1. Free Energy of Passive Permeation of Small Molecule Drugs.** As discussed to a great extent in previous research,[25,45,46,70] since the lipid bilayer is homogeneous and symmetric, the drug/top-leaflet and drug/bottom-leaflet interactions should be identical, [i.e., $W$ (CV1,CV2) = $W(-CV1, -CV2)$]. As a result, the level of the convergence of the free energy calculation could be assessed by the level of symmetry with respect to the center of the membrane (i.e., CV1 = 0; CV2 = 0). The 2D free energy surfaces from each of the five replicas are shown in Figure S3 (ketoprofen is employed as the example drug). Although details of the free energy surface vary from one replica to another, these replicas portray very similar features of the permeation. The level of convergence can further be seen from the inserted figure "average" (average over the free energy surfaces from each replica without symmetrizing), which already naturally holds almost perfect central symmetry. Another commonly adopted method of assessing the level of the convergence of the free energy calculation is to measure how different these independent replicas are as depicted in Figure S4 (ketoprofen is again employed as the example drug); the error bar associated with the two-dimensional free energy surface is mostly between 0−1 kcal/mol, with an average of only 0.22 kcal/mol. Figures S3 and S4 demonstrate that each individual TTMetaD replica is trustworthy, but to take full advantage of the symmetric nature of the system, the final estimate of the free energy of the permeation is computed as the average of the free energies calculated from each replica after they have been symmetrized with respect to the center of the lipid bilayer. The two-dimensional free energy surface of the passive permeation of five small molecule drugs (ketoprofen, naproxen, metoprolol, propranolol, and salicylic acid) through a POPC lipid bilayer is depicted in Figure 2, which is zoomed in from the full-scale version (shown in Figure S5) to highlight the regions where the free energy changes rapidly. The MFEP of the permeation (black curve in Figure 2) is calculated from the string method at zero Kelvin,[55] which represents the predominant pathway over a large number of permeations.

As discussed in section 2.2, the MFEP from the two-dimensional free energy surface (Figure 2) corresponds to $W(R)$ in eq 1 and is depicted in Figure 3, in which only half of the permeation (from outside the lipid bilayer to its center) is shown. The MFEP also demonstrates the correlation between the hydrophobicity of the drug and its permeation dynamics. Shown in Figure 4, a zoomed-in figure of the free energy surface of the permeation of ketoprofen from Figure 2 is an example: the blue-dashed diagonal line (i.e., CV1 = CV2) on the two-dimensional free energy surface indicates the long axis of the drug being parallel to the surface of the bilayer. The

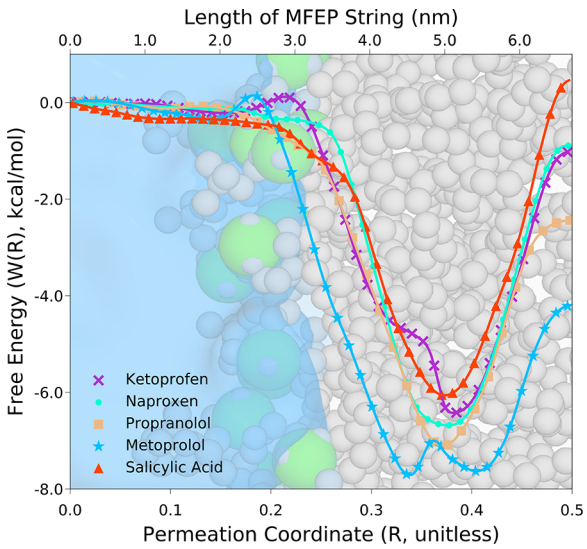


**Figure 3.** Free energy (in kcal/mol) of permeation of five small molecule drugs. The values of the free energy are obtained from the MFEP from the two-dimensional free energy surface in Figure 2. The initial point of MFEP (i.e., $R$ = 0.0) is chosen where the drug is outside the head groups (CV1 and CV2 are less than −4.5 nm). The large green spheres represent the head groups of the bilayer, and the smaller gray spheres represent the tails.

position of the MFEP relative to this diagonal line reveals the orientation of the drug. In the denoted region of the MFEP in Figure 4 (from points a to h), when the drug molecule approaches the lipid bilayer, the MFEP first lies above the diagonal line (i.e., CV1 < CV2). Recall the definition of the CVs in Figure 1: CV1 is the center of mass distance between the carboxyl group (hydrophilic) and the lipid bilayer, while CV2 is the center of mass distance between the benzene group (hydrophobic) and the lipid bilayer. Therefore, the configuration change, a → b, indicates that the head groups of the lipids "pull" ketoprofen closer through the hydrophilic interaction with the carboxyl group. After the carboxyl group further submerges into the head groups (configuration b → c), the benzene group flips from the aqueous phase into the tail groups of the lipid (configurations c → d → e), maximizing the hydrophobic−hydrophobic interaction between them. This flip has reversed the orientation of the drug with respect to the lipid bilayer and has brought the MFEP below the diagonal line (i.e., CV1 > CV2). Through establishing both hydrophilic−hydrophilic (carboxyl/head) and hydrophobic−hydrophobic (benzene/tail) interactions, it results in the global minimal of the free energy at configuration *e*. As the drug moves further into the lipid bilayer (configurations e → f → g → h), this orientation holds in order to minimize the distance between the head groups of the lipids and the carboxyl group of ketoprofen while maintaining the favored hydrophobic interaction between the lipid tails and the benzene group of ketoprofen. It is of interest to note that the free energy change associated with the orientation of ketoprofen, which can be seen as the change in the free energy along the direction orthogonal to the CV1 = CV2 line, is much stronger when the drug is near the head groups as compared to in bulk water and in the lipid tails. This result indicates that ketoprofen is firmly "locked" into the preferred oreintation (configurations *e* and *f* in Figure 4) when it is at the interface between the lipid bilayer and the bulk water. Herein we also clarify the origin of the


https://doi.org/10.1021/acs.jctc.1c00661
J. Chem. Theory Comput. 2022, 18, 503−515

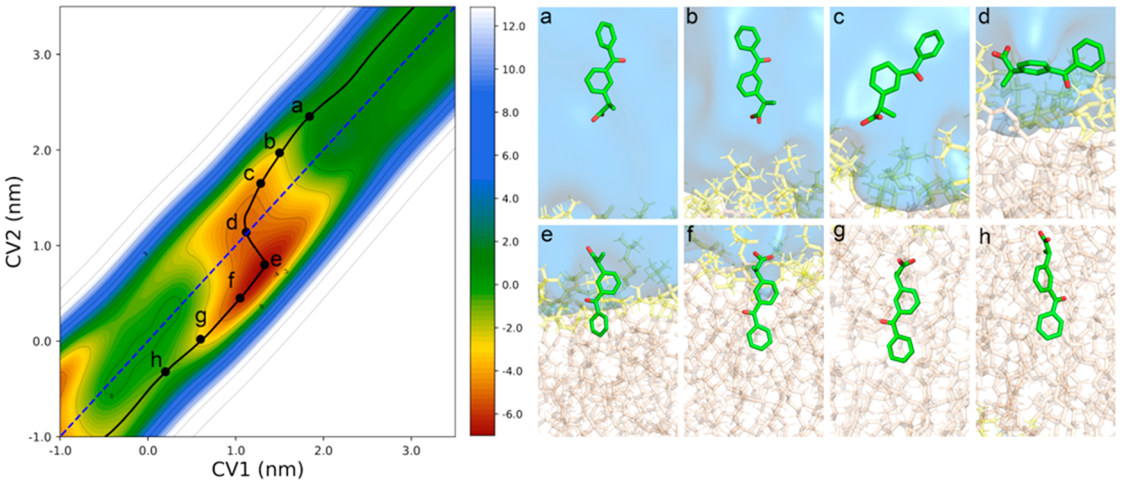


**Figure 4.** A demonstration of the configurations along the MFEP of the permeation of Ketoprofen (zoomed in from Figure 2). The CVs are defined in Figure 1. The diagonal (blue dash) line indicates that the long axis of the drug is parallel to the surface of the membrane. The unit of the free energy is kcal/mol. Ketoprofen is in its neutral form with the hydrogens not depicted explicitly for clarity.

dashed black curve in Figure 2, which is a central symmetric image of the MFEP (solid black curve): the dashed black curve is a result of the artifact of the string method at zero Kelvin.[55] As depicted in Figure S6, the center of the lipid bilayer (i.e., CV1 = 0; CV 2 = 0) is a local maximum on the free energy surface due to the small free energy barrier associated with the change in the orientation of the molecule. Consequently, the MFEP located by the string method at zero Kelvin avoids crossing the center but, instead, finds a path that goes around it to connect the free energy well in the opposite leaflet. As a result, the MFEP itself inherently does not have central symmetry and its central symmetric image (dashed black curve) is just as valid of a path as the MFEP.

The two-dimensional free energy surfaces in Figure 2 also detail the differences in the permeation mechanism as a result of the variations in the structure of small molecule drugs. For example, compared to ketoprofen, naproxen is of similar size and molecular weight, sharing the same hydrophilic functional group for one terminal end (*CV*1) but connecting to a less hydrophobic functional group (ether) in the other terminal end (*CV*2). As a result, the free energy difference associated with the orientation of the drug near the headgroup is not as strong as ketoprofen: there exists a shallower well above the diagonal line, indicating the mildly favored interaction between headgroup and ether oxygen (compared to the strongly favored interaction between headgroup and carboxyl group on the other terminal end). The permeation of propranolol also shows a smaller free energy difference associated with the orientation near the headgroup compared to ketoprofen, though its reasoning is almost opposite: propranolol shares a terminal end with similar hydrophobicity as ketoprofen (naphthalene vs benzene, CV2), but the hydrophilicity of the other terminal end is much weaker (secondary amine vs carbonyl, CV1), decreasing the relative difference between depths of the wells below and above the diagonal line. With regard to metoprolol, both terminal ends show similar hydrophilicity (ether oxygen, CV1; secondary amine, CV2), making them almost equally likely to interact with the head groups of the lipid. Last, the free energy of permeation of salicylic acid is very similar to the permeation of ketoprofen in the sense that the CV1/headgroup's hydrophilic interaction is highly favored. Another feature of the permeation of salicylic acid is its much narrower spread due to it being smallest in size among the five drugs.

**3.2. Free Energy Barrier That Determines the Permeability.** The permeability of ketoprofen computed from eq 1 is shown in Figure 5. It is numerically evaluated with

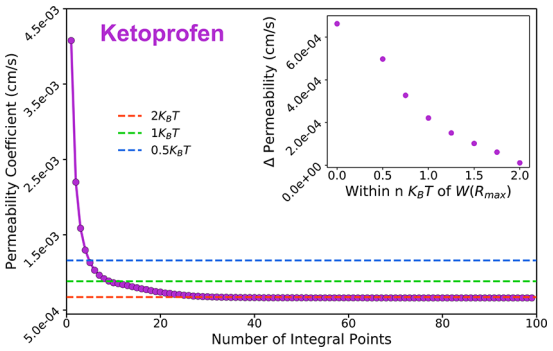


**Figure 5.** The purple line represents the permeability computed from eq 1. The dashed lines denote the permeabilities computed from eq 8 with varying number of $k_BT$ as the cutoff of the integral. The inset figure is the difference in permeability between eq 1 (the asymptotic limit) and eq 8 with differing numbers of $k_BT$.

the trapezoidal rule at 100 discrete points along the MFEP. As stated in the previous section, the diffusivity, $D(R)$, in eq 1 is evaluated through the drug's fluctuation along the MFEP with two-dimensional umbrella samplings. The small molecule drug is first restrained at various positions on the MFEP, and a 100 ns (umbrella) sampling is collected after an equilibration of 100 ns. The evidence provided in the next section shows that the 100 ns (umbrella) sampling is appropriate for the diffusivity calculation. Note that in Figure 5, only a small portion (in this case, about 20%) of the points has a meaningful contribution to the result of the integral. Thus, evaluating the integral numerically for the entire MFEP, which demands the diffusivity calculation of the drug at various positions, is a waste of computational resources. Previous research has shown that the diffusivity of small molecule drugs is about 1 order of magnitude larger in bulk water than it is inside the bilayers, but it varies insignificantly within the lipid bilayers (e.g., as long as the drug is close to the center of the


https://doi.org/10.1021/acs.jctc.1c00661
J. Chem. Theory Comput. 2022, 18, 503−515

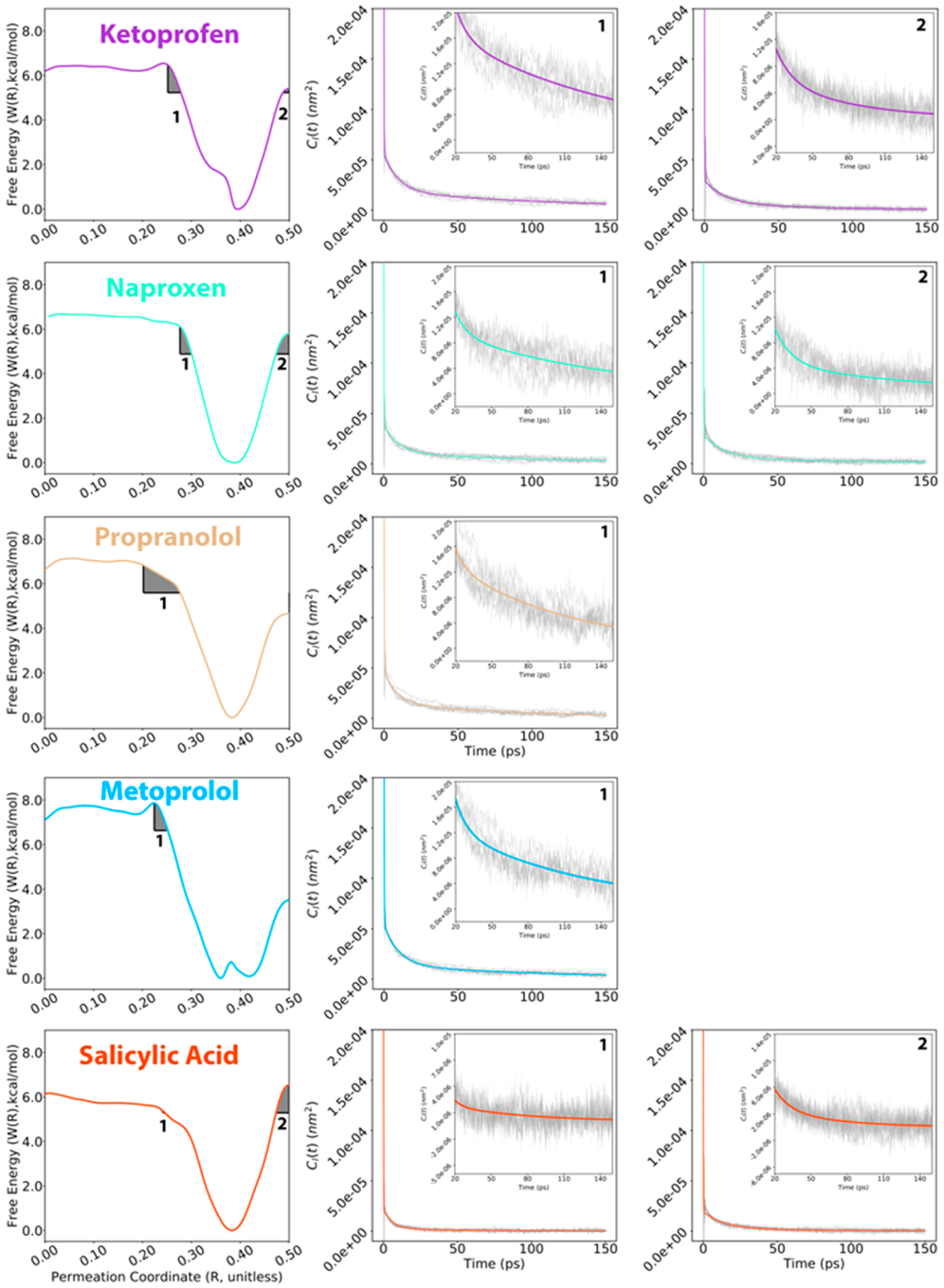


**Figure 6.** Left column: "region of high free energy" for the MFEP integral (eq 8). The bottom of the shaded area shows $2k_BT$ cutoff from the global maximum of the MFEP, which is relevant to the integral of the permeability (eq 8). Note that for some drugs, a second barrier is not necessary. Middle and right columns: autocorrelation function ($C_l(t)$) of small molecule drugs at permeation barriers (1 is the water−bilayer interface and 2 is the center of the lipid). The thin gray lines are $C_l(t)$ of each individual window of 20 ns long. The bold, colored line is the fit of the averaged $C_l(t)$, $C_{l,fit}(t)$.

bilayer, its permeability changes little).[25,45] Further, the exponential factor of $W(R)$ in eq 1 suggests that regions of high free energy along $R$ dominate the integral (and thus the permeability). For example, in the study of the permeation of trimethoprim,[46] the integral over the permeation free energy barrier, which accounts for less than one tenth of the entire permeation path, contributes to more than 90% of the whole integral. Therefore, it is reasonable to expect that the integral of eq 1 is largely dominated by the integral for regions of high free energy.

Before quantitatively defining the "regions of high free energy", it is important to examine the rate-limiting factors of the permeation from the perspective of the free energy. As shown in Figure 3, all five small molecule drugs studied in this manuscript prefer to stay between the water/lipid interface and the bilayer center, corresponding to a $R$ value of ∼0.35. Therefore, starting around $R$ = 0.35, the transition of the drug in either direction would go up against the free energy, which could potentially be rate limiting. Two permeation barriers are present for each drug and they are shown in the left column of


https://doi.org/10.1021/acs.jctc.1c00661
J. Chem. Theory Comput. 2022, 18, 503−515

Figure 6. The water/lipid barrier (denoted with "1") hinders the drug from escaping to the bulk water, while the bilayer center barrier (denoted with "2") hinders the drug from transiting from one leaflet of the bilayer to the other. The relative height of these two barriers varies between drugs, ranging from the water/lipid barrier as dominant (e.g., metoprolol) to two comparable barriers (e.g., salicylic acid). In addition, we note two well-adopted practices from previous studies to further simplify eq 1: the first practice is that a full permeation event initiates when the drug molecule enters into one side of the bilayer and ends when the drug molecule exits from the other side of the bilayer.[25,34,35,45,46] As a result, the transition of a drug in the bulk leading to or following the permeation does not contribute to the permeability. The second practice is that the rate of the transition of the drug in a direction that decreases the free energy is not rate limiting (e.g., ~0.2 → ~0.35, but its mirror image, ~0.65 → ~0.8 is rate limiting).[25,34,35,45,46] As a result, the drug experiences each barrier only once in a full permeation process. Combining these two practices with the existence of multiple barriers, eq 1 could be approximated as

$$\frac{1}{P} = \frac{1}{D(R_{m,1})}\int_{R_{0,1}}^{R_{m,1}} \exp[\beta W(R)]\mathrm{d}R + \frac{1}{D(R_{m,2})}\int_{R_{0,2}}^{R_{m,2}} \exp[\beta W(R)]\mathrm{d}R \quad (8)$$

in which $R_{m,1}$ and $R_{m,2}$ denotes the value of $R$ at the peak of the barrier at the water/lipid interface and the center of the bilayer, respectively (Figure 6). We first determine the range of the integral (the so-called "regions of high free energy"), enclosed by $R_{m,1}$ and $R_{0,1}$ as well as $R_{m,2}$ and $R_{0,2}$, by making sure that the integrals in eq 8 approach the same results of eq 1. The inserted figure of Figure 5 depicted the results of eq 8 in which $R_{0,1}$ and $R_{0,2}$ satisfy:

$$W(R_{0,1}) = W(R_{0,2}) = W(R_{\max}) - n \times k_{\mathrm{B}}T \quad (9)$$

$n$ = 0, 0.5, 1.0, . . . and $W(R_{\max}) = \max(W(R_{m,1}), W(R_{m,2}))$. Figure 5 shows that when only regions within $0.5k_{\mathrm{B}}T$ are included in the integral of eq 8, the permeability is within 75% of the one predicted with the entire integral (eq 1), and as $n$ increases, this agreement gets better. It is also worth noting that eq 8 does not demand both barriers to be rate-limiting. For example, in the case of metoprolol, where $W(R_{m,1})$ is larger than $W(R_{m,2})$ by more than $2k_{\mathrm{B}}T$, the second term in eq 8 vanishes. Overall, applying eq 8 instead of eq 1 to estimate the permeability has decreased the number of diffusivity calculations from tens to just one or two.

**3.3. Permeability of Small Molecule Drugs.** For every small molecule drug (except for metoprolol and propranolol) studied in this manuscript, two diffusivities ($D(R_{m,1})$ and $D(R_{m,2})$) are necessary to estimate its permeability. As discussed in the Methodology section, the drug molecule is held at the respective positions on the MFEP corresponding to $R_{m,1}$ and $R_{m,2}$ by a harmonic potential for 100 ns (i.e., umbrella sampling). These 100 ns MD simulations are evenly divided into five windows, and their variance and autocorrelation function (e.g., $\sigma^2$ ($l$) and $C_l(t)$ in eq 6, respectively) are computed for each window. The configurations of the system (and their corresponding CV values) are recorded every 2 fs. The results of the autocorrelation function from each window are depicted in the middle and right columns of Figure 6. It is obvious that $C_l(t)$ in the denominator of eq 6 is required to converge to zero asymptotically otherwise the integral is not defined. Unfortunately, previous research has reported that it could take up to microseconds for $C_l(t)$ to reach zero.[25] A common workaround of the slow converging autocorrelation function is to integrate $C_l(t)$ from 0 to $t'$ instead of to infinity, in which $C_l(t')$ is 5% of the initial value of $C_l(t)$. In this research, the middle and right columns of Figure 6 indicate that after 150 ps, the values of $C_l(t)$ have decreased to less than 1% of its initial value. Since the focus of this manuscript is not to study the diffusion motion of small molecule drugs in lipid bilayers, but instead, to develop an efficient screening protocol to predict their permeabilities, a summation of three exponentials is chosen to fit the average of the $C_l(t)$ from the aforementioned five windows, i.e.,

$$C_{l,\mathrm{fit}}(t) = \sum_{i=1}^{3} a_i \exp(-b_i t);\ \ a_i,\ b_i \geq 0 \quad (10)$$

$a_i$ and $b_i$ are coefficients chosen to minimize the error between $C_{l,\mathrm{fit}}(t)$ and the average of the $C_l(t)$. The function form of $C_{l,\mathrm{fit}}(t)$ ensures its integral converges and the coefficients are provided in Table S2. The $C_{l,\mathrm{fit}}(t)$ is shown as the bold curve in the middle and right columns of Figure 6 and its integral to infinity replaces the denominator in eq 6.

It is also of importance to demonstrate that the length of the umbrella sampling (i.e., 100 ns) is sufficient to characterize the diffusion motion of the drug at $R_{m,1}$ and $R_{m,2}$. Herein, ketoprofen is selected as a representative case again, and its $D(R_{m,1})$ is calculated with much longer umbrella samplings up to half of a microsecond. The autocorrelation functions and diffusivities calculated from these longer simulations can be found in Figure S7 and Table S3, which indicate that the 100 ns umbrella sampling is sufficient to estimate the diffusivity of the small molecule drugs with reasonable accuracy. The diffusivity and permeability of the five small molecule drugs from eq 8 is summarized in Table 1.

**Table 1. *In silico* Diffusivities and Permeability of the Five Small Molecule Drugs[a]**

| drug | diffusivity $D(R_{m,1})$ ($10^{-7}$ cm$^2$/s) | diffusivity $D(R_{m,2})$ ($10^{-7}$ cm$^2$/s) | permeability ($10^{-6}$ cm/s) |
|---|---|---|---|
| ketoprofen | 5.09 | 16.3 | 674 |
| naproxen | 8.66 | 13.3 | 1530 |
| propranolol | 8.17 | — | 228 |
| metoprolol | 7.21 | — | 91.2 |
| salicylic acid | 48.9 | 32.4 | 2300 |

[a] $2k_{\mathrm{B}}T$ is employed to define the region of integral in eq 8, i.e., $W(R_{0,1}) = W(R_{0,2}) = W(R_{max}) - 2k_{\mathrm{B}}T$. $D(R_{m,2})$ of propranolol and metoprolol is omitted due to the negligible contribution to the integral.

## 4. DISCUSSION

It is of interest to compare the permeability estimated from eq 8 with experimental results. However, identifying a proper experimental benchmark is far from trivial. As summarized in Table 2, the permeability of the same drug can vastly differ from experiment to experiment. For example, the permeability of propranolol ranges between $1.28 \times 10^{-6}$ cm/s (double artificial membrane permeation assay, DAMPA)[73] and $170 \times 10^{-6}$ cm/s (MDCK).[78] The permeabilities show strong assay-dependence (e.g., the artificial membrane assays permeability is


https://doi.org/10.1021/acs.jctc.1c00661
J. Chem. Theory Comput. 2022, 18, 503−515

Table 2. Experimental Permeability of the Five Small Molecule Drugs (Unit: $10^{-6}$ cm/s)[a]

| membrane | intestinal | *in silico* | PAMPA | TPAMPA | DPAMPA |
|---|---|---|---|---|---|
| reference no. | 17,18 | N/A | 71 | 72 | 73 |
| ketoprofen | 870 | 674 | 16.7 | 4.13 | 3.27 |
| naproxen | 850 | 1530 | 10.6 | 6.03 | N/A |
| propranolol | 291 | 228 | 23.5 | 8.64 | 1.28 |
| metoprolol | 134 | 91.2 | 3.5 | 4.29 | 0.65 |
| salicylic acid | N/A | 2300 | 3.3 | N/A | 0.49 |
| membrane | Caco-2 | Caco-2 | Caco-2 | PVPA | MDCK |
| reference no. | 74 | 75 | 76 | 77 | 78 |
| ketoprofen | N/A | N/A | 24.4 | N/A | 20 |
| naproxen | N/A | 42.4[d] | 53.1 | 3.79 | N/A |
| propranolol | 21.8 | 30.6[d] | 47.2 | 1.76 | 170[b] |
| metoprolol | 23.7 | N/A | 31.8 | 1.61 | 150[c] |
| salicylic acid | 22.0 | 19.6[d] | N/A | 0.54 | 10 |

[a]Due to its superiority in indicating the drug's bioavailability, the permeability measured with an intestinal assay was highlighted and employed as a benchmark to compare with the simulation. [b]The dose form is propranolol HCl. [c]The dose form is metoprolol titrate. [d]Average of apical to basolateral and basolateral to apical permeabilities.

usually lower than cell-based membrane assay permeability), but even within the same category of membrane assays, they can still vary significantly. In addition, experiments also show ambiguity in distinguishing whether one small molecule drug is more permeable than another one. For example, in a tri-layer PAMPA study (TPAMPA),[72] Chen et al. reported that naproxen is slightly more permeable than ketoprofen ($6.03 \times 10^{-6}$ cm/s vs $4.13 \times 10^{-6}$ cm/s). In contrast, naproxen is shown to be less permeable than ketoprofen ($10.6 \times 10^{-6}$ cm/s vs $16.7 \times 10^{-6}$ cm/s) with the PAMPA.[71]

Among all the permeabilities summarized in Table 2, since the *in vivo* (i.e., intestinal) measured permeability is the gold standard and correlates best with oral bioavailability,[17,18] it is employed as the benchmark to compare with the *in silico* derived permeabilities. It is important to note that the salicylic acid intestinal permeability has not been measured, thus its benchmark value is not available. It is also important to note that the *in vivo* permeability shown in Table 2 is a measure of the effective intestinal permeability. By definition, the effective permeability contains contributions from all permeation mechanisms, the main ones being, passive paracellular, passive transcellular, and active transcellular. The MD-derived permeability is an *in silico* estimate of the passive transcellular component of the overall effective permeability. Molecules that have a significant paracellular or active transcellular component to permeability would not be expected to correlate with the MD-derived permeability. The compounds in Table 2 are all known to be passive transcellularly absorbed compounds so it is valid to correlate the effective permeabilities of these compounds with the MD-derived permeability as is done here. Summarizing the results, the difference of the value between the permeability from the simulation and intestinal-assay ranges between $43-680 \times 10^{-6}$ cm/s. The permeability predicted from eq 8 is (22% ∼ 32%) smaller than those measured with the intestinal assay, except for naproxen, whose *in silico* permeability is 80% larger than it measured with the intestinal assay. This level of difference might seem large at first sight but should be put into proper perspective by examining the performance of other commonly used methods in assessing the intestinal permeability. In comparison to *in vitro* methods, none of the results from artificial membrane assays or cell-based membrane assays comes close to reproducing the intestinal permeability values. For example, the permeability measured with artificial membrane assays (e.g., PAMPA, TPAMPA, DPAMPA, and PVPA) is about ten to a hundred times (1,000% to 10,000%) smaller, while the permeability measured with cell-based membrane assays (e.g., Caco-2 and MDCK) is on average 12 times (1,200%) smaller. Therefore, the reported *in silico* method has shown significant improvement in predicting intestinal permeability in comparison to *in vitro* methods.

Unfortunately, to our best knowledge, there has not been a single MD-based investigation on the permeability of all these five small molecules. Nonetheless, numerous studies have been carried out on other small organic molecules thus their general performance could be assessed. A detailed review of the efforts of MD-based methods in predicting the permeability of small molecule drugs can be found in a recently published review[22] and herein a few examples of the most relevant studies are listed: C. Lee et al. studied the permeation of urea, benzoic acid, and codeine with a similar solubility−diffusion model (eq 1).[25] The potential of the mean force of the permeation was computed with various enhanced sampling methods (umbrella sampling, replica-exchange, and adaptive biasing force), and the diffusivities were computed with the generalized Langevin approach. The computed permeabilities were reported to be within 1.5 log units (∼3,200%) of the experimental value. In another recent study, B. Bennion et al. investigated the permeation of nine small molecule drugs that were categorized by PAMPA as impermeable or having low-, medium-, or high-permeability.[35] Their simulation successfully put these drugs into these categories, nonetheless, the MD-predicted permeability is still off from the experimental value by roughly 4 log units (1,000,000%). In an effort to study the impact of the composition of the membrane on the permeability of small molecule drugs, M. Palaiokostas et al. studied 13 permeants with MD simulations, which included molecules of similar size such as urea, glycine, and benzoic acid.[79] Their MD permeability accurately represented the experimental permeability of urea (∼0.5 log unit, 316%) but were off from the experimental permeabilities of glycine and benzoic acid by more than 5 log units (10,000,000%). As a summary, it remains very challenging for MD-based permeabilities to be on the same order of magnitude (i.e., one log unit) as the experimental result, therefore, we consider the accuracy of the permeabilities predicted from eq 8 (10%∼65% smaller than those measured with the intestinal-assay) a dramatic improvement from the status quo.

## ■ ASSOCIATED CONTENT

### Supporting Information

The Supporting Information is available free of charge at https://pubs.acs.org/doi/10.1021/acs.jctc.1c00661.

(Figure S1) Ketoprofen's diffusive motion for all five TTMetaD replicas, (Table S1) result of the reparameterization of the partial charges of propranolol, (Figure S2) demonstration of the water-proton donor/acceptor interactions, (Table S2) coefficients for the fit of the average autocorrelation, (Figure S3) two-dimensional free energy surfaces for each replica of ketoprofen, (Table S3) diffusivity of ketoprofen predicted from the



https://doi.org/10.1021/acs.jctc.1c00661
J. Chem. Theory Comput. 2022, 18, 503−515

2D umbrella sampling of differing lengths, (Figure S4) the associated error plot of ketoprofen's two-dimensional free energy surface, (Figure S5) full two-dimensional free energy surface, (Figure S6) zoomed-in two-dimensional free energy surface, highlighting the "central island" of high free energy, (Figure S7) autocorrelation functions calculated from the umbrella samplings of different lengths (PDF)

## AUTHOR INFORMATION


### Corresponding Author

**Rui Sun** − *Department of Chemistry, The University of Hawai'i at Manoa, Honolulu, Hawaii 96822, United States;* orcid.org/0000-0003-0638-1353; Email: ruisun@hawaii.edu

### Authors

**Alyson Shoji** − *Department of Chemistry, The University of Hawai'i at Manoa, Honolulu, Hawaii 96822, United States*

**Christopher Kang** − *Department of Chemistry, The University of Hawai'i at Manoa, Honolulu, Hawaii 96822, United States*

**Kazuumi Fujioka** − *Department of Chemistry, The University of Hawai'i at Manoa, Honolulu, Hawaii 96822, United States*

**John P. Rose** − *DDCS, Lilly Corporate Center, Eli Lilly and Company, Indianapolis, Indiana 46285, United States*

Complete contact information is available at: https://pubs.acs.org/10.1021/acs.jctc.1c00661


### Notes

The authors declare no competing financial interest.

## ACKNOWLEDGMENTS

The authors appreciate the Information and Technology Services (ITS) from the University of Hawai'i, Manoa, and XSEDE for the computational resources. We are grateful to the financial support from Eli Lilly and Company. We would also like to acknowledge the financial support from the University of Hawai'i, including supporting Jackson Hornung, an undergraduate student who helped on this project.

## REFERENCES


(1) Stocks, M. The Small Molecule Drug Discovery Process - from Target Selection to Candidate Selection. In *Introduction to Biological and Small Molecule Drug Research and Development: Theory and Case Studies*; Ganellin, R., Roberts, S., Jefferis, R., Eds. Elsevier: Oxford, 2013; pp 81−126.

(2) White, R. J. The Early History of Antibiotic Discovery: Empiricism Ruled. In *Antibiotic Discovery and Development*; Dougherty, T. J., Pucci, M. J., Eds. Springer US: Boston, MA, 2012; pp 3−31.

(3) Veber, D. F.; Johnson, S. R.; Cheng, H. Y.; Smith, B. R.; Ward, K. W.; Kopple, K. D. Molecular Properties That Influence the Oral Bioavailability of Drug Candidates. *J. Med. Chem.* **2002**, *45* (12), 2615−2623.

(4) Arkin, M. M. R.; Wells, J. A. Small-Molecule Inhibitors of Protein-Protein Interactions: Progressing towards the Dream. *Nat. Rev. Drug Discovery* **2004**, *3* (4), 301−317.

(5) Lennernäs, H.; Abrahamsson, B. The Use of Biopharmaceutic Classification of Drugs in Drug Discovery and Development: Current Status and Future Extension. *J. Pharm. Pharmacol.* **2010**, *57* (3), 273−285.

(6) Pagliara, A.; Reist, M.; Geinoz, S.; Carrupt, P.-A.; Testa, B. Evaluation and Prediction of Drug Permeation. *J. Pharm. Pharmacol.* **2010**, *51* (12), 1339−1357.

(7) Berben, P.; Bauer-Brandl, A.; Brandl, M.; Faller, B.; Flaten, G. E.; Jacobsen, A. C.; Brouwers, J.; Augustijns, P. Drug Permeability Profiling Using Cell-Free Permeation Tools: Overview and Applications. *Eur. J. Pharm. Sci.* **2018**, *119* (April), 219−233.

(8) Volpe, D. A. Drug-Permeability and Transporter Assays in Caco-2 and MDCK Cell Lines. *Future Med. Chem.* **2011**, *3*, 2063−2077.

(9) Irvine, J. D.; Takahashi, L.; Lockhart, K.; Cheong, J.; Tolan, J. W.; Selick, H. E.; Grove, J. R. MDCK (Madin-Darby Canine Kidney) Cells: A Tool for Membrane Permeability Screening. *J. Pharm. Sci.* **1999**, *88* (1), 28−33.

(10) Hubatsch, I.; Ragnarsson, E. G. E.; Artursson, P. Determination of Drug Permeability and Prediction of Drug Absorption in Caco-2 Monolayers. *Nat. Protoc.* **2007**, *2*, 2111.

(11) Kansy, M.; Senner, F.; Gubernator, K. Physicochemical High Throughput Screening: Parallel Artificial Membrane Permeation Assay in the Description of Passive Absorption Processes. *J. Med. Chem.* **1998**, *41* (7), 1007−1010.

(12) Li, C.; Wainhaus, S.; Uss, A. S.; Cheng, K.-C. High-Throughput Screening Using Caco-2 Cell and PAMPA Systems. In *Drug Absorption Studies*; Ehrhardt, C., Kim, K.-J., Eds. Springer US: Boston, MA, 2007; pp 418−429.

(13) Volpe, D. A. Variability in Caco-2 and MDCK Cell-Based Intestinal Permeability Assays. *J. Pharm. Sci.* **2008**, *97* (2), 712−725.

(14) Avdeef, A.; Artursson, P.; Neuhoff, S.; Lazorova, L.; Gråsjö, J.; Tavelin, S. Caco-2 Permeability of Weakly Basic Drugs Predicted with the Double-Sink PAMPA Method. *Eur. J. Pharm. Sci.* **2005**, *24* (4), 333−349.

(15) Di, L.; Kerns, E. H. Permeability Methods. In *Drug-Like Properties*; Di, L., Kerns, E., Eds. Academic Press: Boston, 2016; pp 325−337.

(16) Bischoff, S. C.; Barbara, G.; Buurman, W.; Ockhuizen, T.; Schulzke, J.-D.; Serino, M.; Tilg, H.; Watson, A.; Wells, J. M. Intestinal Permeability − a New Target for Disease Prevention and Therapy. *BMC Gastroenterol.* **2014**, *14* (1), 189.

(17) Dahlgren, D.; Roos, C.; Sjögren, E.; Lennernäs, H. Direct In Vivo Human Intestinal Permeability (Peff) Determined with Different Clinical Perfusion and Intubation Methods. *J. Pharm. Sci.* **2015**, *104* (9), 2702−2726.

(18) Lennernäs, H. Intestinal Permeability and Its Relevance for Absorption and Elimination. *Xenobiotica* **2007**, *37* (10−11), 1015−1051.

(19) Lipinski, C. A.; Lombardo, F.; Dominy, B. W.; Feeney, P. J. Experimental and Computational Approaches to Estimate Solubility and Permeability in Drug Discovery and Development Settings. *Adv. Drug Delivery Rev.* **2001**, *46* (1−3), 3−26.

(20) Lipinski, C. A. Rule of Five in 2015 and beyond: Target and Ligand Structural Limitations, Ligand Chemistry Structure and Drug Discovery Project Decisions. *Adv. Drug Delivery Rev.* **2016**, *101*, 34−41.

(21) Shultz, M. D. Two Decades under the Influence of the Rule of Five and the Changing Properties of Approved Oral Drugs. *J. Med. Chem.* **2019**, *62* (4), 1701−1714.

(22) Venable, R. M.; Krämer, A.; Pastor, R. W. Molecular Dynamics Simulations of Membrane Permeability. *Chem. Rev.* **2019**, *119* (9), 5954−5997.

(23) Tse, C. H.; Comer, J.; Sang Chu, S. K.; Wang, Y.; Chipot, C. Affordable Membrane Permeability Calculations: Permeation of Short-Chain Alcohols through Pure-Lipid Bilayers and a Mammalian Cell Membrane. *J. Chem. Theory Comput.* **2019**, *15* (5), 2913−2924.

(24) Comer, J.; Schulten, K.; Chipot, C. Permeability of a Fluid Lipid Bilayer to Short-Chain Alcohols from First Principles. *J. Chem. Theory Comput.* **2017**, *13* (6), 2523−2532.

(25) Lee, C. T.; Comer, J.; Herndon, C.; Leung, N.; Pavlova, A.; Swift, R. V.; Tung, C.; Rowley, C. N.; Amaro, R. E.; Chipot, C.; Wang, Y.; Gumbart, J. C. Simulation-Based Approaches for

Determining Membrane Permeability of Small Compounds. *J. Chem. Inf. Model.* **2016**, *56* (4), 721−733.
(26) Awoonor-Williams, E.; Rowley, C. N. Molecular Simulation of Nonfacilitated Membrane Permeation. *Biochim. Biophys. Acta, Biomembr.* **2016**, *1858* (7), 1672−1687.
(27) Chipot, C.; Comer, J. Subdiffusion in Membrane Permeation of Small Molecules. *Sci. Rep.* **2016**, *6* (1), 35913.
(28) Fuks, B.; Homblé, F. Permeability and Electrical Properties of Planar Lipid Membranes from Thylakoid Lipids. *Biophys. J.* **1994**, *66* (5), 1404−1414.
(29) Diamond, J. M.; Katz, Y. Interpretation of Nonelectrolyte Partition Coefficients between Dimyristoyl Lecithin and Water. *J. Membr. Biol.* **1974**, *17* (1), 121−154.
(30) Marrink, S. J.; Berendsen, H. J. C. Simulation of Water Transport through a Lipid Membrane. *J. Phys. Chem.* **1994**, *98* (15), 4155−4168.
(31) Torrie, G. M.; Valleau, J. P. Nonphysical Sampling Distributions in Monte Carlo Free-Energy Estimation: Umbrella Sampling. *J. Comput. Phys.* **1977**, *23* (2), 187−199.
(32) Barducci, A.; Bonomi, M.; Parrinello, M. Metadynamics. *Wiley Interdiscip. Rev.: Comput. Mol. Sci.* **2011**, *1* (5), 826−843.
(33) Darve, E.; Rodríguez-Gómez, D.; Pohorille, A. Adaptive Biasing Force Method for Scalar and Vector Free Energy Calculations. *J. Chem. Phys.* **2008**, *128* (14), 144120.
(34) Bochicchio, D.; Panizon, E.; Ferrando, R.; Monticelli, L.; Rossi, G. Calculating the Free Energy of Transfer of Small Solutes into a Model Lipid Membrane: Comparison between Metadynamics and Umbrella Sampling. *J. Chem. Phys.* **2015**, *143* (14), 144108.
(35) Bennion, B. J.; Be, N. A.; McNerney, M. W.; Lao, V.; Carlson, E. M.; Valdez, C. A.; Malfatti, M. A.; Enright, H. A.; Nguyen, T. H.; Lightstone, F. C.; Carpenter, T. S. Predicting a Drug's Membrane Permeability: A Computational Model Validated with in Vitro Permeability Assay Data. *J. Phys. Chem. B* **2017**, *121* (20), 5228−5237.
(36) Oruc, T.; Kucuk, S. E.; Sezer, D. Lipid Bilayer Permeation of Aliphatic Amine and Carboxylic Acid Drugs: Rates of Insertion, Translocation and Dissociation from MD Simulations. *Phys. Chem. Chem. Phys.* **2016**, *18*, 24511.
(37) Shore, P. A.; Brodie, B. B.; Hogben, C. A. The Gastric Secretion of Drugs: A PH Partition Hypothesis. *J. Pharmacol. Exp. Ther.* **1957**, *119* (3), 361−369.
(38) Schanker, L. S.; Tocco, D. J.; Brodie, B. B.; Hogben, C. A. Absorption of Drugs from the Rat Small Intestine. *J. Pharmacol. Exp. Ther.* **1958**, *123* (1), 81−88.
(39) Baptista, A. M.; Teixeira, V. H.; Soares, C. M. Constant-PH Molecular Dynamics Using Stochastic Titration. *J. Chem. Phys.* **2002**, *117*, 4184.
(40) Mertz, J. E.; Pettitt, B. M. Molecular Dynamics At a Constant PH. *Int. J. Supercomput. Appl. High Perform. Comput.* **1994**, *8* (1), 47−53.
(41) Yue, Z.; Li, C.; Voth, G. A.; Swanson, J. M. J. Dynamic Protonation Dramatically Affects the Membrane Permeability of Drug-like Molecules. *J. Am. Chem. Soc.* **2019**, *141* (34), 13421−13433.
(42) Venable, R. M.; Pastor, R. W. Molecular Dynamics Simulations of Water Wires in a Lipid Bilayer and Water/Octane Model Systems. *J. Chem. Phys.* **2002**, *116*, 2663.
(43) Vanommeslaeghe, K.; Hatcher, E.; Acharya, C.; Kundu, S.; Zhong, S.; Shim, J.; Darian, E.; Guvench, O.; Lopes, P.; Vorobyov, I.; Mackerell, A. D. J. CHARMM General Force Field: A Force Field for Drug-like Molecules Compatible with the CHARMM All-Atom Additive Biological Force Fields. *J. Comput. Chem.* **2009**, *31* (4), 671−690.
(44) Dama, J. F.; Rotskoff, G.; Parrinello, M.; Voth, G. A. Transition-Tempered Metadynamics: Robust, Convergent Metadynamics via on-the-Fly Transition Barrier Estimation. *J. Chem. Theory Comput.* **2014**, *10* (9), 3626−3633.
(45) Sun, R.; Han, Y.; Swanson, J. M. J.; Tan, J. S.; Rose, J. P.; Voth, G. A. Molecular Transport through Membranes: Accurate Permeability Coefficients from Multidimensional Potentials of Mean Force and Local Diffusion Constants. *J. Chem. Phys.* **2018**, *149* (7), 072310.
(46) Sun, R.; Dama, J. F.; Tan, J. S.; Rose, J. P.; Voth, G. A. Transition-Tempered Metadynamics Is a Promising Tool for Studying the Permeation of Drug-like Molecules through Membranes. *J. Chem. Theory Comput.* **2016**, *12* (10), 5157−5169.
(47) Laio, A.; Parrinello, M. Escaping Free-Energy Minima. *Proc. Natl. Acad. Sci. U. S. A.* **2002**, *99* (20), 12562−12566.
(48) Sutto, L.; Marsili, S.; Gervasio, F. L. New Advances in Metadynamics. *Wiley Interdiscip. Rev. Comput. Mol. Sci.* **2012**, *2* (5), 771−779.
(49) Laio, A.; Rodriguez-Fortea, A.; Gervasio, F. L.; Ceccarelli, M.; Parrinello, M. Assessing the Accuracy of Metadynamics. *J. Phys. Chem. B* **2005**, *109* (14), 6714−6721.
(50) Barducci, A.; Bussi, G.; Parrinello, M. Well-Tempered Metadynamics: A Smoothly Converging and Tunable Free-Energy Method. *Phys. Rev. Lett.* **2008**, *100* (2), 020603.
(51) Dama, J. F.; Parrinello, M.; Voth, G. A. Well-Tempered Metadynamics Converges Asymptotically. *Phys. Rev. Lett.* **2014**, *112* (24), 1−6.
(52) Crespo, Y.; Marinelli, F.; Pietrucci, F.; Laio, A. Metadynamics Convergence Law in a Multidimensional System. *Phys. Rev. E* **2010**, *81* (5), 055701.
(53) Aydin, F.; Sun, R.; Swanson, J. M. J. Mycolactone Toxin Membrane Permeation: Atomistic versus Coarse-Grained MARTINI Simulations. *Biophys. J.* **2019**, *117* (1), 87−98.
(54) Sun, R.; Sode, O.; Dama, J. F.; Voth, G. A. Simulating Protein Mediated Hydrolysis of ATP and Other Nucleoside Triphosphates by Combining QM/MM Molecular Dynamics with Advances in Metadynamics. *J. Chem. Theory Comput.* **2017**, *13* (5), 2332−2341.
(55) E, W.; Ren, W.; Vanden-Eijnden, E. Simplified and Improved String Method for Computing the Minimum Energy Paths in Barrier-Crossing Events. *J. Chem. Phys.* **2007**, *126* (16), 164103.
(56) Hummer, G. Position-Dependent Diffusion Coefficients and Free Energies from Bayesian Analysis of Equilibrium and Replica Molecular Dynamics Simulations. *New J. Phys.* **2005**, *7*, 34−34.
(57) Woolf, T. B.; Roux, B. Conformational Flexibility of O-Phosphorylcholine and o-Phosphorylethanolamine: A Molecular Dynamics Study Solvation Effects. *J. Am. Chem. Soc.* **1994**, *116* (13), 5916−5926.
(58) Best, R. B.; Zhu, X.; Shim, J.; Lopes, P. E. M.; Mittal, J.; Feig, M.; MacKerell, A. D. Optimization of the Additive CHARMM All-Atom Protein Force Field Targeting Improved Sampling of the Backbone $\varphi$, $\psi$ and Side-Chain X1 and X2 Dihedral Angles. *J. Chem. Theory Comput.* **2012**, *8* (9), 3257−3273.
(59) Jorgensen, W. L.; Chandrasekhar, J.; Madura, J. D.; Impey, R. W.; Klein, M. L. Comparison of Simple Potential Functions for Simulating Liquid Water. *J. Chem. Phys.* **1983**, *79* (2), 926−935.
(60) Parrinello, M.; Rahman, A. Polymorphic Transitions in Single Crystals: A New Molecular Dynamics Method. *J. Appl. Phys.* **1981**, *52* (12), 7182−7190.
(61) Hess, B.; Bekker, H.; Berendsen, H. J. C.; Fraaije, J. G. E. M. LINCS: A Linear Constraint Solver for Molecular Simulations. *J. Comput. Chem.* **1997**, *18* (12), 1463−1472.
(62) Allouche, A. R. Gabedita - A Graphical User Interface for Computational Chemistry Softwares. *J. Comput. Chem.* **2011**, *32* (1), 174−182.
(63) Abraham, M. J.; Murtola, T.; Schulz, R.; Pall, S.; Smith, J. C.; Hess, B.; Lindahl, E. Gromacs: High Performance Molecular Simulations through Multi-Level Parallelism from Laptops to Supercomputers. *SoftwareX* **2015**, *1−2*, 19−25.
(64) Tribello, G. A.; Bonomi, M.; Branduardi, D.; Camilloni, C.; Bussi, G. PLUMED 2: New Feathers for an Old Bird. *Comput. Phys. Commun.* **2014**, *185* (2), 604−613.
(65) Frisch, M. J.; Trucks, G. W.; Schlegel, H. B.; Scuseria, G. E.; Robb, M. A.; Cheeseman, J. R.; Scalmani, G.; Barone, V.; Petersson, G. A.; Nakatsuji, H.; Li, X.; Caricato, M.; Marenich, A. V.; Bloino, J.; Janesko, B. G.; Gomperts, R.; Mennucci, B.; Hratch, D. J.; Frisch, M. J.; Trucks, G. W.; Schlegel, H. B.; Scuseria, G. E.; Robb, M. A.;


https://doi.org/10.1021/acs.jctc.1c00661
J. Chem. Theory Comput. 2022, 18, 503−515

Cheeseman, J. R.; Scalmani, G.; Barone, V.; Petersson, G. A.; Nakatsuji, H.; Li, X.; Caricato, M.; Marenich, A. V.; Bloino, J.; Janesko, B. G.; Gomperts, R.; Mennucci, B.; Hratchian, H. P.; Ortiz, J. V.; Izmaylov, A. F.; Sonnenberg, J. L.; Williams-Young, D.; Ding, F.; Lipparini, F.; Egidi, F.; Goings, J.; Peng, B.; Petrone, A.; Henderson, T.; Ranasinghe, D.; Zakrzewski, V. G.; Gao, J.; Rega, N.; Zheng, G.; Liang, W.; Hada, M.; Ehara, M.; Toyota, K.; Fukuda, R.; Hasegawa, J.; Ishida, M.; Nakajima, T.; Honda, Y.; Kitao, O.; Nakai, H.; Vreven, T.; Throssell, K.; Montgomery, J. A., Jr.; Peralta, J. E.; Ogliaro, F.; Bearpark, M. J.; Heyd, J. J.; Brothers, E. N.; Kudin, K. N.; Staroverov, V. N.; Keith, T. A.; Kobayashi, R.; Normand, J.; Raghavachari, K.; Rendell, A. P.; Burant, J. C.; Iyengar, S. S.; Tomasi, J.; Cossi, M.; Millam, J. M.; Klene, M.; Adamo, C.; Cammi, R.; Ochterski, J. W.; Martin, R. L.; Morokuma, K.; Farkas, O.; Foresman, J. B.; Fox, D. J. *Gaussian 16*, revision C.01.; Gaussian, Inc., Wallin, 2016.

(66) Aikens, C. M.; Webb, S. P.; Bell, R. L.; Fletcher, G. D.; Schmidt, M. W.; Gordon, M. S. A Derivation of the Frozen-Orbital Unrestricted Open-Shell and Restricted Closed-Shell Second-Order Perturbation Theory Analytic Gradient Expressions. *Theor. Chem. Acc.* **2003**, *110* (4), 233−253.

(67) Pritchard, B. P.; Altarawy, D.; Didier, B.; Gibson, T. D.; Windus, T. L. New Basis Set Exchange: An Open, Up-to-Date Resource for the Molecular Sciences Community. *J. Chem. Inf. Model.* **2019**, *59* (11), 4814−4820.

(68) Klauda, J. B.; Venable, R. M.; Freites, J. A.; O'Connor, J. W.; Tobias, D. J.; Mondragon-Ramirez, C.; Vorobyov, I.; Mackerell, A. D., Jr.; Pastor, R. W.; Connor, J. W. O. Update of the CHARMM All-Atom Additive Force Field for Lipids. *J. Phys. Chem. B* **2010**, *114* (23), 7830−7843.

(69) Szabo, A.; Ostlund, N. L. *Modern Quantum Chemistry: Introduction to Advanced Electronic Structure Theory*; Dover Publications: New York, 1996.

(70) Tse, C. H.; Comer, J.; Wang, Y.; Chipot, C. Link between Membrane Composition and Permeability to Drugs. *J. Chem. Theory Comput.* **2018**, *14* (6), 2895−2909.

(71) Zhu, C.; Jiang, L.; Chen, T. M.; Hwang, K. K. A Comparative Study of Artificial Membrane Permeability Assay for High Throughput Profiling of Drug Absorption Potential. *Eur. J. Med. Chem.* **2002**, *37* (5), 399−407.

(72) Chen, X.; Murawski, A.; Patel, K.; Crespi, C. L.; Balimane, P. V. A Novel Design of Artificial Membrane for Improving the PAMPA Model. *Pharm. Res.* **2008**, *25* (7), 1511−1520.

(73) Kataoka, M.; Tsuneishi, S.; Maeda, Y.; Masaoka, Y.; Sakuma, S.; Yamashita, S. A New in Vitro System for Evaluation of Passive Intestinal Drug Absorption: Establishment of a Double Artificial Membrane Permeation Assay. *Eur. J. Pharm. Biopharm.* **2014**, *88* (3), 840−846.

(74) Yazdanian, M.; Glynn, S. L.; Wright, J. L.; Hawi, A. Correlating Partitioning and Caco-2 Cell Permeability of Structurally Diverse Small Molecular Weight Compounds. *Pharm. Res.* **1998**, *15* (9), 1490−1494.

(75) Pade, V.; Stavchansky, S. Link between Drug Absorption Solubility and Permeability Measurements in Caco-2 Cells. *J. Pharm. Sci.* **1998**, *87* (12), 1604−1607.

(76) Alsenz, J.; Haenel, E. Development of a 7-Day, 96-Well Caco-2 Permeability Assay with High-Throughput Direct UV Compound Analysis. *Pharm. Res.* **2003**, *20* (12), 1961−1969.

(77) Naderkhani, E.; Isaksson, J.; Ryzhakov, A.; Flaten, G. E. Development of a Biomimetic Phospholipid Vesicle-Based Permeation Assay for the Estimation of Intestinal Drug Permeability. *J. Pharm. Sci.* **2014**, *103* (6), 1882−1890.

(78) Irvine, J. D.; Takahashi, L.; Lockhart, K.; Cheong, J.; Tolan, J. W.; Selick, H. E.; Grove, J. R. MDCK (Madin-Darby Canine Kidney) Cells: A Tool for Membrane Permeability Screening. *J. Pharm. Sci.* **1999**, *88* (1), 28−33.

(79) Palaiokostas, M.; Ding, W.; Shahane, G.; Orsi, M. Effects of Lipid Composition on Membrane Permeation. *Soft Matter* **2018**, *14*, 8496.



https://doi.org/10.1021/acs.jctc.1c00661
*J. Chem. Theory Comput.* 2022, 18, 503−515